Simultaneous epidural functional Near-InfraRed Spectroscopy and cortical electrophysiology as a tool for studying local...

9 authors, including:

Some of the authors of this publication are also working on these related projects:

Project   Pharmaco-Based fMRI and Neurophysiology in Non-Human Primates View project

Project   Sensory information in continuous brain signals View project

Q1 # Simultaneous epidural functional near-infrared spectroscopy and cortical electrophysiology as a tool for studying local neurovascular coupling in primates

Q2 Ali Danish Zaidi [a,b,*], Matthias H.J. Munk [a], Andreas Schmidt [a,b], Cristina Risueno-Segovia [a], Rebekka Bernard [a], Eberhard Fetz [c,d], Nikos Logothetis [a,e], Niels Birbaumer [b,f,g], Ranganatha Sitaram [b,h,**]

[a] Max Planck Institute for Biological Cybernetics, Tübingen, Germany
[b] Institute for Medical Psychology and Behavioral Neurobiology, University of Tübingen, Germany
[c] Department of Physiology and Biophysics, Washington National Primate Research Center, University of WA, Seattle, USA
[d] Department of Bioengineering, Washington National Primate Research Center, University of WA, Seattle, USA
[e] Center for Imaging Sciences, Biomedical Imaging Institute, University of Manchester, UK
[f] Ospedale San Camillo, Istituto di Ricovero e Cura a Carattere Scientifico, Venezia-Lido, Italy
[g] Department of Psychology, Biological Psychology, Universidad de las Islas Baleares, Spain
[h] Department of Biomedical Engineering, University of Florida, Gainesville, FL, USA

ARTICLE INFO

ABSTRACT

Simultaneous measurements of intra-cortical electrophysiology and hemodynamic signals in primates are essential for relating human neuroimaging studies with intra-cortical electrophysiology in monkeys. Previously, technically challenging and resourcefully demanding techniques such as fMRI and intrinsic-signal optical imaging have been used for such studies. Functional near-infrared spectroscopy is a relatively less cumbersome neuroimaging method that uses near-infrared light to detect small changes in concentrations of oxy-hemoglobin (HbO), deoxy-hemoglobin (HbR) and total hemoglobin (HbT) in a volume of tissue with high specificity and temporal resolution. fNIRS is thus a good candidate for hemodynamic measurements in primates to acquire local hemodynamic signals during electrophysiological recordings. To test the feasibility of using epidural fNIRS with concomitant extracellular electrophysiology, we recorded neuronal and hemodynamic activity from the primary visual cortex of two anesthetized monkeys during visual stimulation. We recorded fNIRS epidurally, using one emitter and two detectors. We performed simultaneous cortical electrophysiology using tetrodes placed between the fNIRS sensors. We observed robust and reliable responses to the visual stimulation in both [HbO] and [HbR] signals, and quantified the signal-to-noise ratio of the epidurally measured signals. We also observed a positive correlation between stimulus-induced modulation of [HbO] and [HbR] signals and strength of neural modulation. Briefly, our results show that epidural fNIRS detects single-trial responses to visual stimuli on a trial-by-trial basis, and when coupled with cortical electrophysiology, is a promising tool for studying local hemodynamic signals and neurovascular coupling.

© 2015 Published by Elsevier Inc.

Introduction

Simultaneous measurements of intra-cortical electrophysiology and functional neuroimaging are essential for relating the vast array of human neuroimaging studies with the extensive body of primate electrophysiology, which is unlikely to be obtained by using either technique in isolation (Logothetis et al., 2001). Such measurements in primates have Q3 previously been performed by combining cortical electrophysiology either with fMRI (Goense and Logothetis, 2008; Pauls et al., 2001) or intrinsic signal optical imaging (ISOI) (Cardoso et al., 2012; Sirotin and Das, 2009). Using fMRI, one can obtain a 3D map of the hemodynamic activations in the brain, albeit at a low sampling rate (~1 Hz). The challenges for combining fMRI with cortical electrophysiology include interference compensation and correction of the gradient noise, apart from the relatively large monetary investment. ISOI has the advantage of both high spatial resolution and high sampling rate of hemodynamic signals above a region of the cortex. However, in order to perform ISOI on primates, the dura above the region of interest (ROI) needs to be removed, sometimes being replaced by a transparent silicone membrane. This

perturbation of the dura is a potential source of infection. Combining ISOI with electrophysiology is also a challenge, as the electrode drive can be a hindrance to the imaging, significantly reducing the number of electrodes that can be used in tandem (Sirotin and Das, 2009). A less explored, and far less expensive approach for measurement of hemodynamic signals in primates is functional near-infrared spectroscopy (fNIRS).

fNIRS is a non-invasive neuroimaging method that uses a near-infrared light source and detector pair (optode pair), to measure changes in concentrations of oxy-hemoglobin (HbO), deoxy-hemoglobin (HbR) and total hemoglobin (HbT) in a small volume of tissue (Ferrari and Quaresima, 2012). The advantages of fNIRS include its portability, metabolic specificity, high temporal resolution, high sensitivity in detecting small substance concentrations, affordability and low susceptibility to movement artifacts (Kohl-Bareis et al., 2002; Villringer and Chance, 1997). Typically, fNIRS is measured from optodes fixed on the scalp, where it is subjected to spurious signals from hemoglobin concentration changes in the scalp tissue. The cortical hemodynamic signals are severely dampened by those originating from the scalp tissue, and most often the underlying cortical responses are only retrieved after rigorous signal averaging (Saager et al., 2011). One way to circumvent the problem is to record fNIRS signals from directly above the dura, after removing the scalp and bone. This would bring the optodes very close to the region of interest, with more infrared light illuminating the cortical tissue, eventually leading to a higher signal-to-noise ratio (SNR). Under these circumstances, fNIRS could be a very sensitive technique for hemodynamic measurements in primates, specifically to measure local neurovascular signals during electrophysiological recordings.

In this study, we tested the sensitivity of epidural fNIRS and the feasibility of combining epidural fNIRS with recording from microelectrodes in neocortex. We recorded hemodynamic and neuronal activity from the primary visual cortex in two anesthetized monkeys during visual stimulation. We developed a plastic chamber inset that housed optodes and guide tubes arranged in a linear fashion (Fig. 1A) to enable us to position the optodes and electrodes close to each other, and hence, record both types of signals simultaneously from a small volume of cortical tissue. We observed clear, strong trial-by-trial activations in the [HbO] and [HbR] signals that were correlated with the underlying cortical neural activation. These results demonstrate that epidurally measured fNIRS signals have high SNR, and when combined with cortical electrophysiology, provide a highly reliable and sensitive method for studying local neurovascular-coupling.

## Methods

Surgery and craniotomy

Two healthy adult rhesus monkeys, M1 (female; 8 kg) and M2 (male; 10 kg), were used for experiments. Vital parameters were monitored during anesthesia. After sedation of the animals using ketamine (15 mg/kg), anesthesia was initiated with fentanyl (31 μg/kg), thiopental (5 mg/kg) and succinylcholine chloride (3 mg/kg), and then the animals were intubated and ventilated. A DatexOhmeda Avance (GE, USA) was used for ventilation, with respiration parameters adjusted to maintain an end-expiratory CO_2 of 4.0%. Anesthesia was maintained with remifentanil (0.5–3 μg/kg/min) and eye movements were prevented by mivacurium chloride (4–7 mg/kg/h). Depending on the blood pressure, an iso-osmotic solution (Jonosteril, Fresenius Kabi, Germany) or a plasma expander (Volulyte, Fresenius Kabi, Germany) was infused at a rate of ~10 (5–15) ml/kg/h. During the entire experiment, body temperature was carefully regulated between 38.5 °C and 39.5 °C, and SpO_2 was maintained above 95%. Under anesthesia, a small skin cut and craniotomy were made above the left hemisphere in order to access the primary visual cortex (V1). In all subsequent experiments, the bone opening was cleaned from connective tissue exposing the dura for insertion of microelectrodes. For each monkey, at least two weeks were allowed for recovery between successive experiments. All experiments were approved by the local authorities (Regierungspräsidium, Tübingen) and are in agreement with guidelines of the European Community for the care of laboratory animals.

Positioning of optodes and electrodes

To enable precise positioning of electrodes relative to the optodes, we developed a cylindrical plastic chamber inset (Fig. 1A) that rested on the skull of the monkey around the craniotomy. The bottom of the inset was molded to the curvature of the skull so that it fit snugly on the bone. The inset had three large vertical holes of 2.5 mm diameter each, spaced 6 mm apart, arranged linearly (Fig. 1B). These holes were used to hold the NIRS optodes. The optodes protruded approximately 5 mm from the lower surface of the plastic inset (Fig. 1A) so as to touch the dural surface. Out of these three optodes, one peripheral optode was used as an emitter and two optodes were used as detectors. The emitter–detector pair that was separated by 6 mm was called the 'near' channel, and the emitter detector pair separated by 12 mm was called the 'far' channel.

Between the optode holes, there were two rows of three smaller holes, linearly aligned, measuring 0.4 mm in diameter, for holding the guide tubes with tetrodes and/or single electrodes inside (Fig. 1B). Each of these holes was 1.2 mm apart from the other, and the two rows were separated by a distance of 1 mm from the center. The guide tubes also protruded approximately 5 mm from the lower surface of the inset. The inset, housing the optodes and electrodes was then lowered on to the craniotomy using a stereotactic manipulator. After correct positioning was confirmed, we began driving the electrodes into the cortex. During the recording, the most medial optode served as the emitter and the others served as detectors. Halfway into the
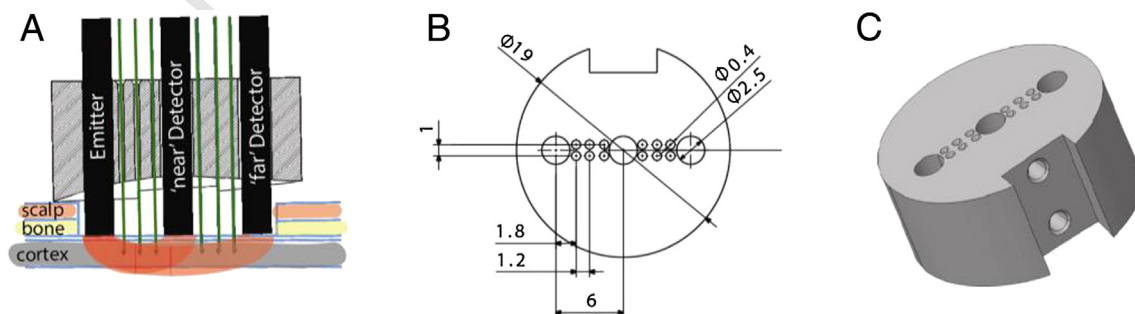
Fig. 1. Schematic representation of plastic inset with the optodes and electrodes in position. (A) Vertical section through the plastic inset showing the relative position of optodes (black cylinders) and tetrodes (blue arrows pointing downwards). The scalp and bone were removed during surgery and the optodes were lowered on the dura. The guide tubes of the tetrodes also rested on the dura. The tetrodes were driven into the cortex. (B) A top-view of the plastic inset showing the relative positions of optodes and electrodes, and the diameters of the holes. The three large, central holes are for optodes and the twelve small holes between them are for guide tubes for holding and driving electrodes. The holes on the lower edge are for screws to help stabilize the fNIRS optodes. All values are in millimeters. (C) 3D rendering of the plastic inset with the holes for optodes and electrodes aligned linearly in the center. The two holes on the front face were used for screws to attach the inset to the Thomas Recording Matrix head.

session, the position of the emitter was exchanged, so that the most lateral optode became the emitter and the others become the detectors. The central optode was always used as the 'near' detector.

fNIRS measurement

For fNIRS measurements, we used a NIRScout machine (NIRx Medizintechnik GmbH, Berlin), which performs dual wavelength LED light-based spectroscopic measurements at 760 and 850 nm. Sampling was performed at 20 Hz. We used modified emitters and detectors, and optical fiber bundles for sending the light from the LED source into the tissue, and also for detecting refracted light from the tissue. Both the emitter and detector fiber bundles had iron ferrule tips with an aperture of 2.5 mm on the ends that touched the dura. The recording instrument was connected via USB to a laptop computer running an interactive software (NIRStar, NIRx Medizintechnik, GmbH, Germany) provided along with the instrument. The software was used for starting and stopping recordings, and also for setting up the various recording parameters, such as the number of sources and detectors, and the sampling rate. The instrument received TTL pulses from the stimulus system and the electrophysiological recording system for synchronization. The system sent 1-ms TTL pulses every 50 ms to the recording system that corresponded to light pulses. After correct positioning of optodes on to the dura, a gain calibration for the signal was performed.

Electrophysiology

We used custom-built tetrodes and electrodes. All tetrodes and single electrodes had impedance values less than 1 (range, 0.2–0.8) MΩ. The impedance of each channel was noted before loading the tetrodes onto the drive, and once again during unloading after the experiment, to ensure that all contacts were intact throughout the duration of the experiment. To drive the electrodes into the brain we used a 64-channel matrix (Thomas Recording GmbH, Giessen, Germany). The electrodes were loaded in guide tubes a day before the experiment. The output was connected to a speaker and an oscilloscope, with a switch to help cycle between different channels. We advanced electrodes into the cortex one by one until we heard a reliable population response to a rotating checkerboard flickering at 0.5 Hz, left the electrode to relax the tissue and checked tens of minutes later to see how stable the recording was.

Visual stimulation

A fundus camera was used to locate the fovea of each eye. For presenting visual stimulation, a fiber optic system (Avotec, Silent Vision, USA) was positioned in front of each eye, so as to be centered on the fovea. To adjust the plane of focus, contact lenses (hard PMMA lenses, Wöhlk, Kiel, Germany) were inserted to each eye. We used a whole-field, rotating checkerboard to drive the neural activity. The direction of rotation was reversed every second. Each trial consisted of 5 s of visual stimulation followed by 15 s of a dark screen. A single run consisted of 20 trials. Data presented are from 14 runs spread over 8 experimental days.

Data analysis

All analyses were performed in MATLAB using custom-written code. The runs that failed to elicit any significant modulation in the MUA band were excluded from the analysis. Also, only runs that cleared visual screening for artifacts were used.

fNIRS signal processing

The raw wavelength absorption data from the NIRS system were converted to concentration changes of [HbO] and [HbR] using a modified Beer–Lambert equation (Villringer and Chance, 1997). For correlating hemodynamic signals with neural activity, the signals were band-pass filtered between 0.01 and 5 Hz to remove low-frequency drifts and high-frequency noise. The major discernible sources of physiological noise in the NIRS signals are from respiration and pulse. The pulse artifact varies between 1.1 and 2 Hz, The respiration artifact, on the other hand, has a much higher power, and hence contributes more significantly to the variance of the signal. This artifact peaks at 0.1 or 0.09 Hz (corresponding to respiration cycles lasting 10 or 11 s). Although filtering the signal between 0.01 and 1 Hz would remove the pulse artifact, it would not remove the respiration artifact. The respiration artifact can only be removed either by filtering the signal below 0.09 Hz, or by using notch filters at 0.1 and 0.09 Hz. However, both of these procedures could also lead to a loss of information in the signal corresponding to other features, for example, the HbO initial dip (Fig. 2D).

Since the change in [HbR] was negative, the peak-amplitudes for [HbR] are thus also negative. For a trial-by-trial analysis, the hemodynamic response for each trial was zero-corrected by subtracting, from each hemodynamic response, the value at the start of the trial.

Calculation of SNR of hemodynamic signals

We obtained power spectral densities for the [HbO] and [HbR] signals for each run. To calculate the raw SNR, we divided the peak power with the mean power for each run.

Electrophysiological signal processing

The raw broadband signal was sampled at 20.8333 kHz. From the raw signal, the multiunit activity (MUA; 1000–3000 Hz) was filtered out. The envelope of the MUA was then obtained by taking the absolute value of the Hilbert transform of the filtered signal. The band-envelope was then converted to standard deviation units by subtracting the mean and dividing by the standard deviation of the signal. The modulation index (MI) for each trial was calculated using the formula $MI = (MUA_{On} - MUA_{Off})/(MUA_{On} + MUA_{Off})$; where MUA_{On} is the mean MUA activity during the On epoch and MUA_{Off} is the mean MUA power during the Off epoch for each trial.

Statistics

All significance values are based on Wilcoxon's signed rank test on the various distributions of hemodynamic and neuronal activity, such as [HbO] and [HbR] peak-amplitudes and peak-time, and the neural modulation index. Standard error of means is reported along with all mean values in the text. In the figures, the shaded regions represent 95% confidence intervals.

Results

Single trial responses in [HbO] and [HbR] in an example run

We observed reliable responses to visual stimulation manifested as changes in the concentrations of both HbO and HbR on a trial-by-trial basis. Fig. 2A shows the [HbO] and [HbR] signals for an example run. The mean value has been subtracted from each signal. As can be clearly seen, during each On epoch the [HbO] signal begins to rise after a small delay (~1 s). It peaks around 7 s, and then begins to fall again, returning to the baseline value. The [HbR] follows a similar time-course, albeit inverted. Although there is some variability in the peak-amplitudes of the [HbO] for each trial, the strong response to the visual stimulation for each trial shows the sensitivity of epidural fNIRS and its high SNR (see Section 3.2 for details on SNR). The [HbO] and [HbR] signals had larger peak-amplitude and lesser noise for the 'near' emitter–detector pair (6 mm distance) compared to the 'far' (12 mm distance) (Table 1; Fig. 3B), and hence data from only the 'near' pair are shown. A strong pulse artifact with a periodicity of ~1.4 Hz was also observed in the fNIRS signals as small but regular peaks in the [HbO] (Fig. 2C).
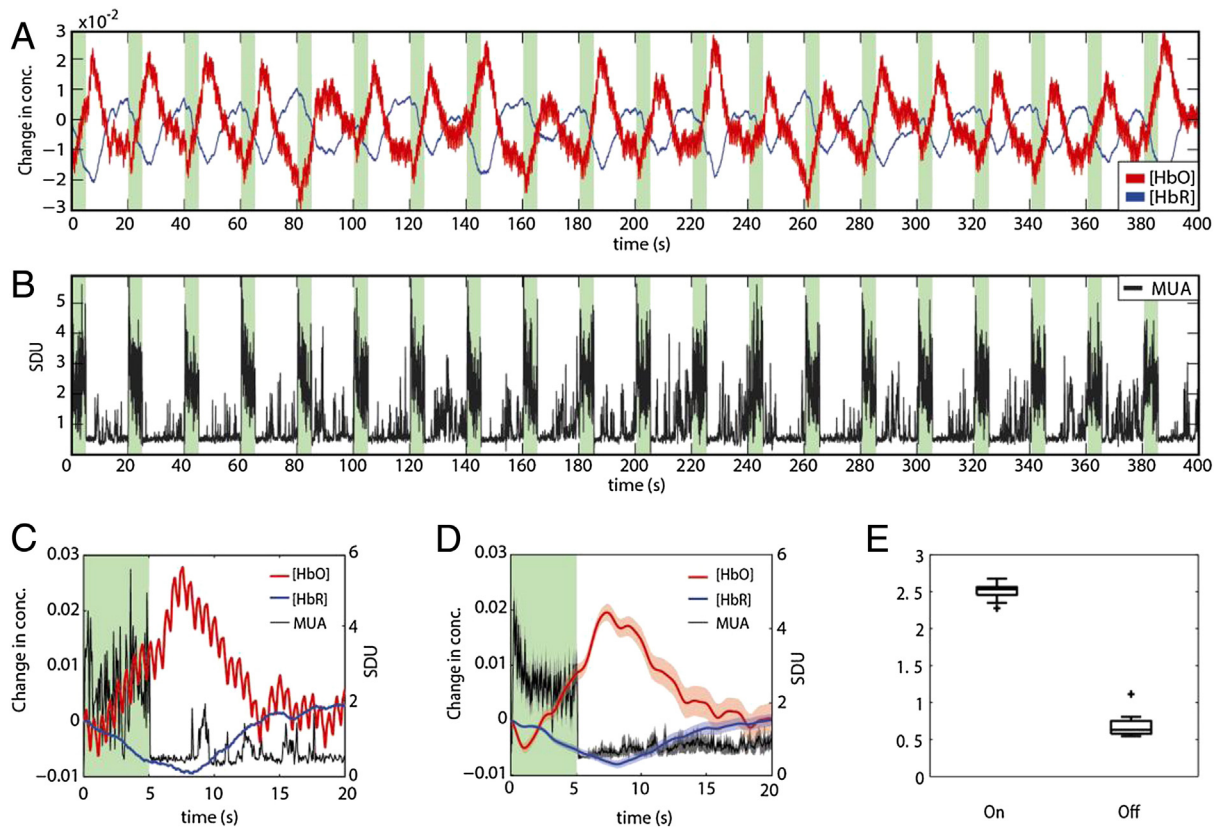
Fig. 2. Data from example run consisting of 20 trials. (A) Raw, unfiltered signals of changes in concentrations in HbO (red) and HbR (blue) from an example run. The On (green) and Off (white) epochs were 5 and 15 s, respectively, repeating 20 times. The x-axis represents time in seconds. The means have been subtracted from both signals. Strong trial-by-trial activations can be clearly observed in both signals. (B) Band-envelope of the MUA (1–3 kHz) signal for the run as Fig. 1A. The signal was standardized by subtracting the mean and dividing by the standard deviation, and the minimum value was subtracted. The y-axis represents standard deviation units, the x-axis represents time in seconds. (C) The first 20 s of the [HbO], [HbR] and MUA signals plotted in A and B. The pulse artifact in the [HbO] signal is clearly visible. (D) The mean [HbO], [HbR] and MUA signals obtained after averaging the 20 trials in A and B. Each trial was zero-corrected (the value at the beginning of the trial was set to zero). The shaded regions represent 95% confidence intervals. (E) Distribution of mean MUA values during 20 On and Off epochs shown in B. The means of the two distributions are significantly different ($p < 10^{-8}$; Wilcoxon rank-sum test).

Fig. 2D shows the mean [HbO] and [HbR] signals over the 20 trials of the run. The shaded regions represent 95% confidence intervals.

Fig. 2B plots the MUA activity (in SDU) as a function of time for the same run, showing clear responses to the visual stimuli. The distribution of mean activity during each On and Off epoch is shown in Fig. 2E. The modulation index (MI) for each trial was calculated by obtaining the mean MUA activity during the On and Off epochs of each trial, and applying the formula $MI = (MUA_{On} - MUA_{Off})/(MUA_{On} + MUA_{Off})$; where MUA_{On} is the mean MUA activity during the On epoch and MUA_{Off} is the mean MUA power during the Off epoch. The median of the MI for the 20 trials was significantly greater than zero (mean MI for 20 trials is 0.6, $p < 10^{-4}$; Wilcoxon signed rank test).

Raw signal-to-noise ratio

We estimated the raw signal-to-noise ratio of [HbO] and [HbR] signals during visual stimulation. To calculate SNR, we obtained the pow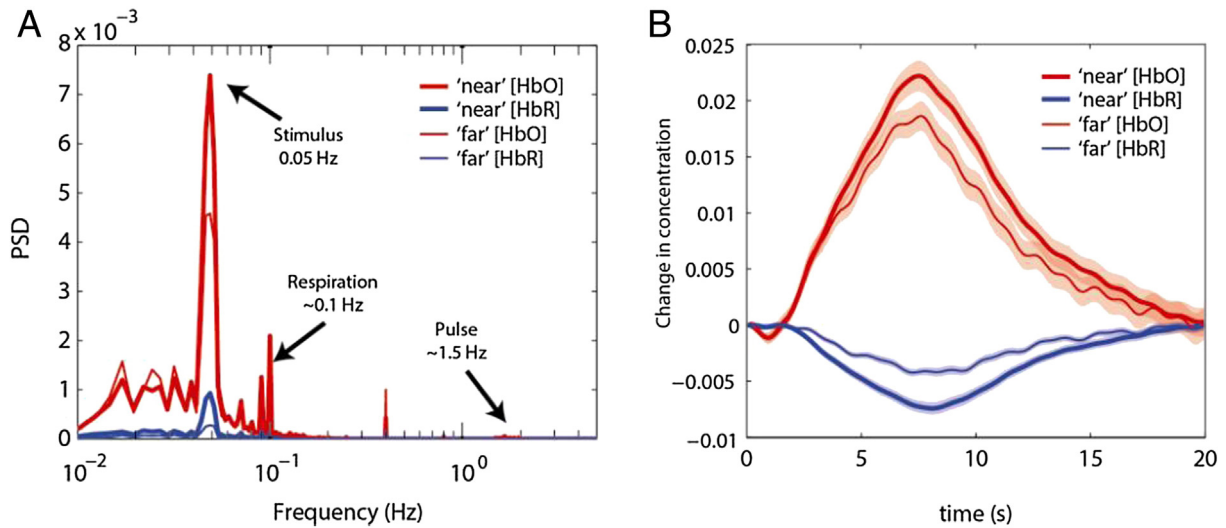er spectral density (PSD) for the [HbO] and [HbR] signals for each run. For every run, the peak in the PSD was around 0.05 Hz (0.0479 ± 0.0005), corresponding to the 20 s trial length (Fig. 3A shows the mean PSD for the 14 runs; data averaged over both monkeys). We refer to the peak-amplitude of the PSD corresponding to the visual modulation as P_{stim}. The 'near' P_{stim} was higher than the 'far' P_{stim} for both [HbO] and [HbR] signals ($p < 10^{-4}$; Wilcoxon signed rank test), showing that the signal modulation was higher in the 'near' channel than the 'far' channel. Also, the P_{stim} for [HbO] was larger than the P_{stim} for [HbR], for both 'near' and 'far' channels (Fig. 3A, thick versus thin traces).

To obtain the SNR for each run, we divided the P_{stim} by the mean power for that run. Table 1 summarizes the SNR distributions for all 14 runs. The mean SNRs for 'near' channel were larger than those from the 'far' channel for both [HbO] and [HbR] signals, but were not significantly different (based on Wilcoxon rank sum test). However, the mean HRF peak-amplitude for the 'near' channel was significantly larger than that for the 'far' channel for both [HbO] and [HbR] signals (Fig. 3B; $p < 10^{-3}$ for all trials over 14 runs; see Supplementary Figure 1 for comparison of 'near' and 'far' channels of a single trial).

The fact that the highest peak in the PSD corresponds to the periodicity of visual stimulation, combined with very high SNR for the signals demonstrates the sensitivity of epidurally measured fNIRS signals.

Hemodynamic responses to visual stimulation

Fig. 4A shows the distributions of peak-amplitude and peak-time for each trial for both [HbO] and [HbR] for both monkeys. The left panel represents the distribution of peak-amplitudes, and the right

Table 1
Raw SNR values for [HbO] and [HbR] signals from the 'near' and 'far' channels.

Parameter	Mean	SEM	Significance*
'near' [HbO]	1078.1	76.4	$p < 10^{-3}$
'near' [HbR]	1057.7	93.7	$p < 10^{-3}$
'far' [HbO]	914.6	55.2	$p < 10^{-3}$
'far' [HbR]	889.2	57.7	$p < 10^{-3}$

* Based on the Wilcoxon signed rank test.

Fig. 3. PSD of [HbO] and [HbR] and corresponding SNR. The thick and thin traces correspond to the 'near' and 'far' channels, and the [HbO] and [HbR] traces are colored red and blue, respectively. (A) The mean power spectral density as a function of frequency. Mean of 14 runs from 2 monkeys. The strongest modulation is around 0.05 Hz, which corresponds to the frequency of visual simulation. Artifacts from respiration and pulse are also marked. (B) The mean HRF obtained by averaging overall trials from all runs for both monkeys. The peak-amplitudes in the 'near' channel are larger for those in the 'far' channel.

panel represents the distribution of peak-time. The [HbO] peak-amplitudes and peak-times for M1 and M2 are shown in Table 2. The absolute values of peak-amplitudes for [HbO] signals were larger than those for the [HbR] signals for both monkeys. Also, the time to peak for the [HbO] was sooner than the time to peak for the [HbR].

Correlations with neuronal activity

In order to determine how the fNIRS signals were related to underlying neuronal activity, we determined whether the [HbO] peak-time was correlated with the MUA MI (Fig. 4B). We obtained the average MI and peak-time for each run. There is a clear and significant correlation between the MI and [HbO] peak-time ($r = 0.65$; $p = 0.011$). A similar relationship was observed between MI and [HbR] ($r = 0.71$; $p = 0.004$). We found stronger correlations between [HbR] peak-time and MI, probably because the [HbR] is less susceptible to biological artifacts caused by breathing and the pulse, both of which are much more obvious in the [HbO] signals (Fig. 2C and 2D). We also found

stronger correlations for [HbO] and [HbR] peak-time than the peak-amplitude (Supplementary Figure 2).

Discussion

Comparison with earlier studies

Epidural fNIRS has been acquired in rats (Crespi, 2007; Crespi et al., 2005) without, and in monkeys (Fuster et al., 2005) with combined electrophysiological recordings. The Crespi studies have shown that epidural fNIRS reliably represents tissue oxygenation changes, but neuronal activity was not recorded. Fuster et al. conducted a study combining epidural fNIRS with ECoG, but did not document the SNR of the fNIRS signals or their correlations with ECoG signals. A device for studying neurovascular coupling in humans based on intracranial acquisition of hemodynamic and neuronal signals has also been developed for diagnostic evaluation for surgical therapy in epilepsy patients (Keller et al., 2009). However, these studies do not quantify
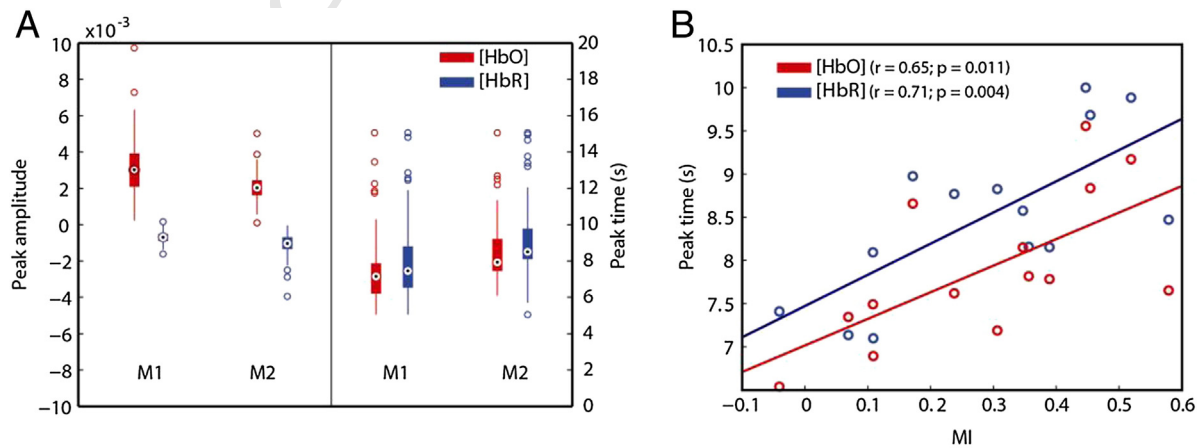
Fig. 4. Distribution of peak-amplitudes and peak-times for all sessions, and their neuronal correlates. (A) The distribution of the peak-amplitude (left panel) and peak-time (right panel) for both [HbO] and [HbR] for each monkey for each trial. For each boxplot, the circle with the black dot represents the median, the thick and thin lines represent the 67% and 95% confidence intervals, respectively, and the hollow circles represent the outliers. The data represent 280 trials recorded over 14 runs. For values refer to Table 1. (B) Neural modulation (MI; *x*-axis) versus the peak-time for the [HbO] and [HbR] (*y*-axis). There is a significant correlation between MI and [HbO] and [HbR] peak-time. Each data point is an average over the 20 trials for each run.

Table 2
Distribution of 'peak-amplitude' and 'peak-time' for [HbO] and [HbR] responses.

Monkey	Parameter	Mean	SEM	Significance*
M1	[HbO] peak-amplitude	0.0309	0.0014	$p < 10^{-20}$
	[HbO] peak-time	7.2842	0.1505	$p < 10^{-20}$
	[HbR] peak-amplitude	−0.0107	0.0005	$p < 10^{-20}$
	[HbR] peak-time	7.7767	0.1727	$p < 10^{-20}$
M2	[HbO] peak-amplitude	0.0206	0.0005	$p < 10^{-27}$
	[HbO] peak-time	8.3737	0.1115	$p < 10^{-27}$
	[HbR] peak-amplitude	−0.0071	0.0002	$p < 10^{-27}$
	[HbR] peak-time	9.0716	0.1282	$p < 10^{-27}$

* Based on Wilcoxon signed rank test.

the sensitivity of invasively acquired fNIRS signals, nor do they check for a relationship with the underlying neuronal activity. We performed simultaneous epidural fNIRS and cortical electrophysiological recordings in two anesthetized macaques during visual stimulation. We observed robust trial-by-trial activations represented as changes in [HbO], [HbR] and neuronal activity in both monkeys. The raw SNR for both [HbO] and [HbR] signals was very high, and the mean peak-time for the hemodynamic response for each run correlated significantly with the mean MUA modulation.

Correlations with neuronal activity

We found significant correlations between hemodynamic peak-time with the underlying neuronal modulations, but not for the peak-amplitude (see Supplementary Figure 1). One of the reasons could be the lack of dynamic range in the stimulus intensity, since we only used a high-contrast rotating checkerboard as a visual stimulus. This may lead to reduction in the dynamic range of the hemodynamic signal. However, on a trial-to-trial basis, the peak-amplitude may also be affected by other processes, for example, the trend of the signal before trial onset. If the oxygen concentration in the tissue is high, and close to saturation, the dynamic range of the signal might be reduced, and smaller peaks in the hemodynamic response might be observed. Instead, if the tissue oxygen concentration is low, the dynamic range of the hemodynamic signal could be high, leading to higher peaks. The slope of the signal before trial onset may influence the tissue saturation, and consequently, signal amplitude. If the signal trend affects the dynamic range of the [HbO] signal, with rising signals decreasing the dynamic range, then the peak-amplitude of the hemodynamic response should be negatively correlated with the slope before trial-onset (see Supplementary Figure 3). The amplitude of the hemodynamic signal has also been reported to depend non-linearly on the underlying neuronal activity (Franceschini et al., 2008), and signal amplitude has been shown to depend on the relationship between the different frequency bands of the electrophysiological signal (Magri et al., 2012). Any or all of the above reasons could influence the peak-amplitude, and hence distort its relationship with the neuronal MI. The reasons for the same are currently being investigated.

Limitations

Near-infrared light is incapable of penetrating deep into brain tissue, and hence the acquisition of fNIRS signals is not possible from deeper brain structures such as the thalamus, superior colliculus, substantia nigra, etc. (Ferrari and Quaresima, 2012). Also, the spatial resolution of fNIRS signals is within millimeters. Therefore, this technique is only applicable for measuring hemodynamic changes of cortical tissue close to the dural surface, with a spatial resolution in millimeters. The exact spatial resolution of fNIRS is currently being investigated.

Conclusions

Overall, our results show that epidural fNIRS is a reliable and sensitive method for studying local hemodynamic changes. We also obtained high SNRs for both [HbO] and [HbR] signals recorded from both the 'near' and the 'far' channels. Lastly, we observed strong visual modulation in the [HbO] and [HbR] signals that, and the hemodynamic modulation was strongly correlated with the underlying neural activity. The current work establishes that simultaneous epidural-fNIRS-electrophysiology is a relatively cheap yet sensitive method for studying neurovascular coupling in primates.

Uncited reference

Sulzer et al., 2013

Appendix A. Supplementary data

Supplementary data to this article can be found online at http://dx.doi.org/10.1016/j.neuroimage.2015.07.019.

References

Cardoso, M.M.B., Sirotin, Y.B., Lima, B., Glushenkova, E., Das, A., 2012. The neuroimaging signal is a linear sum of neurally distinct stimulus- and task-related components. Nat. Neurosci. 15, 1298–1306. http://dx.doi.org/10.1038/nn.3170.

Crespi, F., 2007. Near-infrared spectroscopy (NIRS): a non-invasive in vivo methodology for analysis of brain vascular and metabolic activities in real time in rodents. Curr. Vasc. Pharmacol. 5, 305–321.

Crespi, F., Bandera, A., Donini, M., Heidbreder, C., Rovati, L., 2005. Non-invasive in vivo infrared laser spectroscopy to analyse endogenous oxy-haemoglobin, deoxy-haemoglobin, and blood volume in the rat CNS. J. Neurosci. Methods 145, 11–22. http://dx.doi.org/10.1016/j.jneumeth.2004.11.016.

Ferrari, M., Quaresima, V., 2012. A brief review on the history of human functional near-infrared spectroscopy (fNIRS) development and fields of application. Neuroimage 63, 921–935. http://dx.doi.org/10.1016/j.neuroimage.2012.03.049.

Franceschini, M.A., Nissilä, I., Wu, W., Diamond, S.G., Bonmassar, G., Boas, D.A., 2008. Coupling between somatosensory evoked potentials and hemodynamic response in the rat. Neuroimage 41 (2), 189–203. http://dx.doi.org/10.1016/j.neuroimage.2008.02.061.

Fuster, J., Guiou, M., Ardestani, A., Cannestra, A., Sheth, S., Zhou, Y., Toga, A., Bodner, M., 2005. Near-infrared spectroscopy (NIRS) in cognitive neuroscience of the primate brain. 26 pp. 215–220. http://dx.doi.org/10.1016/j.neuroimage.2005.01.055.

Goense, J.B.M., Logothetis, N.K., 2008. Neurophysiology of the BOLD fMRI signal in awake monkeys. Curr. Biol. 18, 631–640. http://dx.doi.org/10.1016/j.cub.2008.03.054.

Keller, C.J., Cash, S.S., Narayanan, S., Wang, C., Kuzniecky, R., Carlson, C., Devinsky, O., Thesen, T., Doyle, W., Sassaroli, A., Boas, D.A., Ulbert, I., Halgren, E., 2009. Intracranial microprobe for evaluating neuro-hemodynamic coupling in unanesthetized human neocortex. J. Neurosci. Methods 179, 208–218. http://dx.doi.org/10.1016/j.jneumeth.2009.01.036.

Kohl-Bareis, M., Obrig, H., Steinbrink, J., Malak, J., Uludag, K., Villringer, A., 2002. Noninvasive monitoring of cerebral blood flow by a dye bolus method: Separation of brain from skin and skull signals. J. Biomed. Opt. 7, 464–470. http://dx.doi.org/10.1117/1.1482719.

Pauls, J., Augath, M., Trinath, T., Logothetis, N.K., Oeltermann, A., 2001. Neurophysiological investigation of the basis of the fMRI signal. Nature 412, 150–157. http://dx.doi.org/10.1038/35084005.

Saager, R.B., Telleri, N.L., Berger, A.J., 2011. Two-detector corrected near infrared spectroscopy (C-NIRS) detects hemodynamic activation responses more robustly than single-detector NIRS. Neuroimage 55, 1679–1685. http://dx.doi.org/10.1016/j.neuroimage.2011.01.043.

Sirotin, Y.B., Das, A., 2009. Anticipatory haemodynamic signals in sensory cortex not predicted by local neuronal activity. Nature 457, 475–479. http://dx.doi.org/10.1038/nature07664.

Sulzer, J., Haller, S., Scharnowski, F., Weiskopf, N., Birbaumer, N., Blefari, M.L., Bruehl, A.B., Cohen, L.G., DeCharms, R.C., Gassert, R., Goebel, R., Herwig, U., LaConte, S., Linden, D., Luft, A., Seifritz, E., Sitaram, R., 2013. Real-time fMRI neurofeedback: Progress and challenges. Neuroimage 76, 386–399. http://dx.doi.org/10.1016/j.neuroimage.2013.03.033.

Villringer, A., Chance, B., 1997. Non-invasive optical spectroscopy and imaging of human brain function. Trends Neurosci. 20, 435–442.